Available online at www.sciencedirect.com

ScienceDirect

Procedia CIRP 13 (2014) 249 – 256

www.elsevier.com/locate/procedia

2nd CIRP Conference on Surface Integrity (CSI)

The prediction of machined surface hardness using a new physics-based material model

R. Liu[a], M. Salahshoor[a], S.N. Melkote[a,]*, T. Marusich[b]

[a]*Georgia W. Woodruff School of Mechanical Engineering, Georgia Institute of Technology, Atlanta, GA 30332, USA*
[b]*Third Wave Systems, Minneapolis, MN 55344, USA*
* Corresponding author. Tel.: +1-404-894-8499; fax: +1-404-894-9342.*E-mail address*: shreyes.melkote@me.gatech.edu.

Abstract

This paper investigates the prediction of machined surface hardness, a key material property, as a direct consequence of machining induced microstructure evolution. To this end, a new physics-based material model is implemented into the AdvantEdge™ software via a user-defined material subroutine and used to simulate the orthogonal cutting of OFHC copper. This material model explicitly integrates the microstructure, represented by dislocation density and grain size, into the constitutive description of inelastic deformation. The associated microstructure evolution laws in conjunction with the constitutive law provide a unified microstructure-property framework in which the microstructure evolves during deformation via hardening, dynamic recovery, and dynamic recrystallization mechanisms and the evolved microstructure features are directly fed back to the flow stress model. The predicted hardness distribution in the spatial domain of deformation in orthogonal cutting is benchmarked against experimental data.

Keywords: hardness; microstructure; cutting; simulation

1. Introduction

Hardness is a surface integrity metric that significantly affects the in-service performance of machined parts, especially wear resistance. It is one of the most commonly used quantities to assess the mechanical property of manufactured parts. During chip formation, the workpiece material undergoes severe plastic deformation (SPD) during which grain refinement [1,2] and phase transformation [3,4] can occur depending on the type of material, cutting geometry (e.g. rake angle), and process parameters (e.g. depth-of-cut). As a consequence of such metallurgical alterations, the material hardness will change, resulting in a measurable difference between the near surface hardness and the bulk material. Indeed, microhardness measurements have been widely used to identify such metallurgical alterations. The hardness can also evolve when metallurgical alterations are absent simply due to strain hardening caused by dislocation production and storage during SPD. In order to satisfy quality requirements which warrant superior in-service performance, it is essential to investigate the effect of cutting parameters on hardness evolution in the machined surface. In this context, numerical models enabling the hardness prediction for various combinations of cutting parameters are necessary to perform quality-informed design of the cutting process in a time and cost efficient manner.

The material model, describing the constitutive behavior of a material during deformation, is a key component of any numerical simulation that is conducted to parametrically investigate a cutting process. Indeed, the choice of material model profoundly affects the fidelity of predictions. The prediction accuracy depends on the amount of underlying deformation physics that is captured in the material model, particularly when the model is extrapolated outside its calibration range, which is often the case in

doi:10.1016/j.procir.2014.04.043

machining simulations. The Johnson-Cook (JC) model [5] is a widely-used constitutive model in machining simulations. This model is an example of a purely *phenomenological* model wherein the underlying microscale deformation mechanisms and the microstructure evolution during plastic deformation are not explicitly accounted for. The Zerilli-Armstrong (ZA) model [6, 7] is another widely used constitutive model in machining simulations. The ZA model is an example of a *semi-phenomenological* model that is motivated by dislocation mechanics based arguments; however, it does not explicitly account for the evolution of microstructure and its effect on the flow stress during deformation.

Noting that the *initial* hardness has a major influence on the strain hardening response of AISI 52100 bearing steel, Umbrello et al. [8] developed a phenomenological hardness-based flow stress model to simulate the orthogonal cutting of the bearing steel. They assumed the hardness to be independent of plastic work and unaffected by the high temperature in the shear zone. However, the invariance of hardness during machining does not seem to be justified considering other experimental observations of severe grain refinement, phase transformation, and even hardness evolution in the machined surface reported in the literature [3,4]. Later, Umbrello and Filice [9] and Umbrello [10] introduced two phenomenological hardness evolution laws, named *quenching* and *tempering*, to be used in conjunction with the aforementioned hardness-based flow stress model. This model was further enhanced by Caruso et al. [11] to trace the grain size evolution via a Zener-Hollomon parameter (Z) based relationship reported by Yanagimoto et al. [12] (i.e. $D = D_0\beta Z^m$; where β and m are constants and D_0 is the initial grain size). According to this relationship, dynamic recrystallization (DRX) occurs whenever the equivalent plastic strain is larger than a critical strain (ε_{cr}) defined as $\varepsilon_{cr} = \varsigma\sqrt{D_0}Z^n$ where ς and n are constants. However, the grain size still does not have any explicit effect on the flow stress.

Rotella et al. [13] used the same relationship as Caruso et al. to capture the DRX in dry turning of AA7075-T651 alloy. Additionally, they applied a Hall-Petch type relation reported by Hughes et al. [14] (i.e. $H = C_0 + C_1/\sqrt{D}$; where C_0 and C_1 are constants) to trace the hardness evolution as a result of grain refinement. The latter clearly indicates that the hardness is seen as a microstructure dependent characteristic. Also, a Zener-Hollomon parameter based flow stress model reported by Sheppard et al. [15] (i.e. $Z = A(\sinh \alpha\sigma)^n$ where A, α, and n are constants) was used as the constitutive law. As a result, the strain and microstructure dependence of flow stress is neglected in this model. Pu et al. [16] also adopted the Yanagimoto model for DRX along with the Johnson-Cook model for flow stress to simulate the microstructure evolution in dry and cryogenic machining of AZ31B magnesium alloy.

To capture more of the underlying microscale deformation mechanisms and potentially improve the predictive capability of the material model, Ding and Shin [17] adopted the dislocation based material model developed by Estrin et al. [18] and Tóth et al. [19] (*ET model*) to simulate the chip formation and grain refinement in orthogonal cutting of commercially pure Ti (cp-Ti). However, a key limitation of the ET model is that it assumes the existence of an established dislocation cell structure prior to deformation and consequently is only strictly valid for dislocation cell forming materials that have undergone sufficient straining for a cell structure to develop [20]. Moreover, the cell/grain size in the ET model is formulated in a manner that tacitly indicates the occurrence of cell/grain refinement even in the absence of dynamic recrystallization if the hardening and dynamic recovery mechanisms are able to cause a net increase in total dislocation density.

Svoboda et al. [21] adopted the physics based plasticity model developed by Lindgren et al. [22] to simulate the orthogonal cutting of 316L stainless steel alloy. This model was based on the dislocation glide mechanism and the flow stress was formulated as the summation of resistance to dislocation motion imposed by short- (*thermal stress*) and long- (*athermal stress*) range obstacles. The dislocation density and vacancy concentration were taken as internal state variables (ISVs) and the flow stress was expressed as an explicit function of these microstructure-based ISVs in the Lindgren model. In addition, the evolution of ISVs with inelastic deformation was captured via two evolution equations. However, no evolution equation was derived for the grain size, which is indicative of the absence of dynamic recrystallization (DRX) or otherwise the limitation of the Lindgren model in capturing the effects of DRX.

In this paper, a new *physics-based* material model, developed by the authors [23], is utilized to predict the machining induced hardness of OFHC copper. This model explicitly incorporates microstructure evolution due to hardening, dynamic recovery, and dynamic recrystallization into the constitutive law describing the macroscale plastic deformation response of the material over the range of strains, strain rates and temperatures experienced in machining. The unified model is implemented in AdvantEdge^{TM} via a user-defined material subroutine. Orthogonal cutting cases are simulated and model predictions for cutting forces and the machining induced hardness evolution in OFHC copper are compared against experimental data reported in the literature.

2. The physics-based unified material model

The physics-based unified material model developed by the authors is briefly presented in this section. Further details of the model can be found elsewhere [23]. According to the thermal activation theory [24], the flow stress can be formulated as the superposition of an athermal (σ_a) and a thermal (σ_{th}) component as follows:

$$\sigma = \sigma_a + \sigma_{th} \tag{1}$$

The magnitude of σ_{th} depends on the strength of interactions between mobile dislocations and short-range barriers (e.g. interstitial impurities, substitutional alloying elements, precipitates, other dislocations, and even lattice friction). This stress component is formulated using the Kocks and Mecking (KM) model [25,26] as follows:

$$\sigma_{th} = \left[1 - \left(\frac{kT}{g_0 \mu b^3} Ln\left(\frac{\dot{\varepsilon}_0}{\dot{\varepsilon}}\right)\right)^{1/q}\right]^{1/p} \sigma_0 \tag{2}$$

Where, k is the Boltzmann's constant, T is the temperature, g_0 is the normalized activation energy at 0 K, μ is the shear modulus, b is the magnitude of the Burgers vector, $\dot{\varepsilon}_0$ is a reference strain rate, σ_0 is the stress required to overcome short range obstacles at 0 K, and p and q are parameter's defining the shape of energy barriers associated with short range obstacles. The variation of the shear modulus μ with temperature is modeled using Eqn. (3) [27] as follows:

$$\mu = \mu_0 - \sqrt{a + (T/T_r)^2} \tag{3}$$

Where μ_0 is the shear modulus at 0 K and a and T_r are material constants. The athermal component of flow stress is derived from the interaction of mobile dislocations with long range obstacles such as grain boundaries and dislocation forests. This component is formulated in Eqn. (4) as the sum of stresses required to overcome the strain fields of dislocation forests, σ_ρ, and grain boundaries, σ_G, by an individual dislocation:

$$\sigma_a = \sigma_\rho + \sigma_G = \alpha_\rho \, \mu \, b \sqrt{\rho} + \alpha_G \mu \sqrt{\frac{b}{D}} \tag{4}$$

Here α_ρ and α_G are taken as constant parameters related to the strength of dislocation-dislocation forest and dislocation-grain boundary interactions. The ISVs, ρ and D, evolve during inelastic deformation and knowing their values at each strain increment, the flow stress can be calculated by superposing the thermal and athermal components as indicated by Eqn. (1).

The evolution law for dislocation density is derived as follows:

$$\rho_{H\,\&\,DRV} = \left[\frac{A}{B} + \left(\sqrt{\rho_0} - \frac{A}{B}\right) exp\left(-\frac{B\varepsilon}{2}\right)\right]^2 \tag{5}$$

In the above equation, A and B are the *hardening* (due to dislocation production) and *recovery* (due to dislocation annihilation) parameters, respectively. Additionally, ρ_o is the initial dislocation density and $\rho_{H\&DRV}$ is an intermediate dislocation density determined by the competing hardening and dynamic recovery processes. Following Estrin and Mecking [28], A was considered to be a constant and B to be a temperature and strain rate dependent term as follows:

$$B = \left(B_1(T) + B_2(\dot{\varepsilon})\right)^{B_3(T)} \tag{6}$$
$$B_1 = b_0 + b_1 T \tag{7}$$
$$B_2 = b_2 \log_{10} \dot{\varepsilon} \tag{8}$$
$$B_3 = b_3 + b_4 T \tag{9}$$

To capture the grain size evolution during inelastic deformation, the following phenomenological model is introduced:

$$D = D_f + \left(D_0 - D_f\right) \tanh\left(\frac{\varepsilon_r}{\varepsilon}\right)^u \tag{10}$$

where ε_r is the critical strain at which DRX occurs, u is a temperature and strain rate dependent fitting parameter controlling the DRX rate, D_o is the initial grain size, and D_f is the final recrystallized grain size:

$$\varepsilon_r = \varepsilon_0(\log_{10} \dot{\varepsilon} + \varepsilon_1) e^{(\varepsilon_2 / T^{\varepsilon_3})} \tag{11}$$
$$u = u_0(\log_{10} \dot{\varepsilon} + u_1)^{u_2} e^{(u_3 / T^{u_4})} \tag{12}$$
$$D_f = 10^{(C_z - m \log_{10} Z)} \tag{13}$$

Where ε_i (i = 0…3), u_j (j = 0…4), C_z and m are fitting parameters. The Zener-Hollomon parameter (Z) in Eqn. (13) is defined as follows:

$$Z = \dot{\varepsilon} e^{\left(\frac{Q}{RT}\right)} \tag{14}$$

Where Q is the activation energy for lattice self-diffusion and R is the gas constant. During DRX, dislocations are also consumed to form new grain boundaries and, therefore, besides σ_G, the dislocation density and associated strengthening component (σ_ρ) are impacted. In this study, the DRX-induced change in dislocation density is assumed to be proportional to the change in grain surface area per unit volume (S) as follows:

$$\Delta\rho_{DRX} = -K(\dot{\varepsilon}, T)\Delta S = K(\dot{\varepsilon}, T)\left[\frac{2}{D_0} - \frac{2}{D}\right] \tag{15}$$

$$K = (K_0 + K_1 T)(\log_{10} \dot{\varepsilon} + K_2)^{(K_3 + K_4 T)} \quad (16)$$

Where K is a proportionality parameter defining the saturation stress level (where hardening, dynamic recovery, and dynamic recrystallization are in equilibrium) and K_j (j = 0…4) are fitting parameters. The proposed unified material model was calibrated for OFHC copper and then validated for a wide range of temperatures (room temperature up to ~ 550 ^{o}C) and strain rates (quasi-static, 0.0004/s, up to dynamic, 6000/s, loading) using stress vs. strain data. Table 1 lists the values of model parameters for OFHC copper.

Table 1. Unified model parameters for OFHC copper.

Parameter	Value	Parameter	Value
D_0 [μm]	62	b_1 [1/K]	-4.87×10^{-5}
ρ_0 [m^{-2}]	10^{10}	b_2	2.51×10^{-3}
μ_0 [GPa]	47.10	b_3	-0.671
a [GPa^2]	0.14	b_4 [1/K]	-8.06×10^{-5}
T_r [K/GPa]	60.16	ε_0	0.243
b [m]	2.57×10^{-10}	ε_1	9.5
α_G	0.86	ε_2	-1.863×10^{-8}
$\dot{\varepsilon}_0$ [1/s]	2×10^{10}	ε_3	-2.696
p	2/3	u_0	5.809×10^{-3}
q	2.0	u_1	20.26
σ_0 [MPa]	46	u_2	2.278
$k/g_0\mu b^3$ [1/K]	5×10^{-5}	u_3	1.4×10^{-5}
α_ρ	0.5	u_4	-1.768
Q [kJ/mol]	146.04	K_0 [1/m]	5.616×10^{18}
C_z	2.64	K_1 [1/m/K]	-68.27×10^{15}
m	0.17	K_2	10
A [1/m]	6.8×10^{8}	K_3	-9.528
b_0	0.052	K_4 [1/K]	9.079×10^{-3}

3. Hardness vs. flow stress relationship

The hardness prediction in this study is based on the well-known idea that the hardness, H, must be directly proportional to an equivalent uniaxial flow stress, σ_{in}, named *indentation stress*, as follows [30]:

$$H\left[\frac{kg}{mm^2}\right] = C.\sigma_{in} \quad (17)$$

where C is a dimensionless, proportionality constant. In order to compute the σ_{in} at any given location in the spatial domain of deformation field, the microstructure (D, ρ) and deformation (ε, $\dot{\varepsilon}$, T) parameters in the constitutive law, i.e. $\sigma = \sigma(D, \rho; \varepsilon, \dot{\varepsilon}, T)$ in its generic form, should be picked properly to replicate the indentation-induced deformation and attendant microstructure evolution. In that sense, the cutting-induced average grain size, dislocation density, and equivalent uniaxial strain at any given material point will constitute the pre-existing material condition with respect to the ensuing indentation process. Since the indentation process is not expected to result in DRX and further grain refinement, the cutting-induced grain size was used in the constitutive law to calculate the σ_{in} at each material point. In contrast, indentation-induced strain hardening due to the associated dislocation production and storage is expected to be large enough to be detectable. Therefore, the application of cutting-induced dislocation density in σ_{in} calculation appears to be flawed and it necessitates the estimation of indentation-induced dislocation density. To that end, the equivalent uniaxial strain in the dislocation density evolution law, i.e. Eqn. (5), should be substituted with the sum of cutting-induced and indentation-induced strains. The latter is reported to be 8 ~ 10 % based on actual measurements [31]. Here, it is noteworthy that the likely uncertainty in the indentation-induced strain measurement is not expected to result in noticeable discrepancy between the computed and measured hardness values in the chip or machined surface, where the cutting-induced strain is generally quite large (>> 1.0) compared to the indentation-induced strain. However, the discrepancy due to uncertainty propagation is expected to be noticeable in certain regions of the deformation field, for instance near the primary shear zone, where the cutting-induced strain gradually evolves to amounts that are comparable in magnitude to the indentation-induced strain. Additionally, for the purpose of σ_{in} calculation, it was assumed that indentation occurs at the quasi-static rate of 0.1/s and an ambient temperature of 25 ^{o}C.

The next step in using Eqn. (17) to predict the cutting-induced hardness is to determine the value of proportionality constant C. This constant has historically been selected to be 3.0. However, a comparison of the measured and calculated hardness values for annealed copper, reported by Tabor [31] and reproduced in Table 2, reveals that there is a discrepancy between the measurements and calculations for total strains less than 33%. This discrepancy grows larger as the total strain becomes smaller. This is an indication that the constancy of C is not a valid assumption in the entire range of strains experienced by a material in SPD. The latter is confirmed by Chaudhri [32] who noted that the ratio of measured hardness to flow stress, i.e. C in Eqn. (17), was strain-variant for annealed copper when $\varepsilon < 0.2$. However, for $\varepsilon \geq 0.2$, the ratio was approximately constant at ~3.25 depending on the indentation strain. An implication of the foregoing discussion is that keeping C constant may affect the accuracy of the cutting-induced hardness predictions, albeit to a small

extent, in the chip or machined surface, where the strains are well in excess of 1.0. However, the negative influence of C being constant is anticipated to be more pronounced near the primary shear zone, where the cutting-induced strain gradually evolves to strains as large as 20~33%. To avoid such inaccuracy and in the light of the foregoing discussion, a mathematical relation given by Eqn. (18) was developed for the proportionality parameter C. This relation fits the empirical data reported in Table 2 at small strains (ε < 33%) and asymptotically approaches a constant value of ~3.2 for large strains (ε > 33%) (*see* Figure 1).

$$C = \frac{H}{Y} = 2.6 + 0.54 \times (1 - e^{-4.52\,\varepsilon})^{0.41} \qquad (18)$$

Table 2. Empirically measured and calculated hardness values for annealed copper reported by Tabor [31]; Note that the total strain is the sum of pre-strain (ε_0) and indentation strain (i.e. 8%).

Initial Strain ε_0	Total strain $\varepsilon = \varepsilon_0$+0.08	Yield Stress @ εY (kg/mm^2)	3.0×Y	Hardness (kg/mm^2)
0	0.08	15	*45*	*39*
0.06	0.14	20	*60*	*58*
0.12	0.20	23.3	*70*	*69*
0.18	0.26	25	*75*	*76*
0.25	0.33	26.6	*80*	*81*

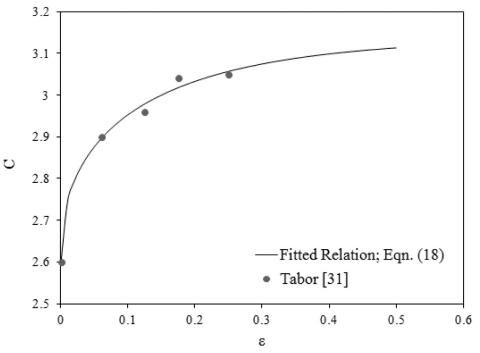

Fig. 1. The illustration of fitted relation, Eqn. (18), to empirical data. Note that the empirical data represented by solid circles are calculated using measured hardness (H) and yield stress (Y) from Table 2 for different amounts of pre-strain.

4. Orthogonal cutting model

A user-defined material subroutine was developed using the FORTRAN language to implement the calibrated unified material model in AdvantEdge^{TM}. This subroutine was further modified to include the hardness vs. flow stress relation. A standard Lagrangian formulation combined with a fully automatic adaptive remeshing algorithm was used to simulate chip formation without any chip separation criterion. The integrated automatic remeshing provides a dense array of refined mesh in the vicinity of the cutting edge accommodating severe deformation gradients in that region. Since the cutting tool was much harder than Cu, it was assumed to be rigid. The cutting edge radius was taken as 20 μm. Additionally, the tool was fixed in both directions and the workpiece was constrained to move horizontally at the specified cutting speed. The width of cut along the cutting edge was taken to be much larger than the depth-of-cut to establish plane strain conditions. The Coulomb law was used to model the frictional contact at the tool/chip interface. The simulated cut length (L=15mm) was long enough to establish steady state conditions. Constrained by the high computation cost, the minimum element size was limited to about 0.02 mm. To evaluate the performance of the model in predicting the cutting-induced hardness, orthogonal cutting simulations of OFHC copper (99.99% pure) and ETP grade copper (99.9% pure), for which data is available in the literature [33,34], were carried out (*see* Table 3). Cutting test No. 1 was conducted on a lathe equipped using quick stop equipment, tubular ETP grade Cu specimen, and Silicon Nitride based ceramic inserts without any cutting fluid. The cutting forces were measured using a three component piezoelectric dynamometer. Cutting test No. 2 was conducted on cylindrical OFHC grade Cu specimen, and a high speed steel tool (clearance angle +10^o). The tool cutting edge was ground using an aluminum oxide grinding wheel (grit size 46) prior to the cutting test. The friction coefficient, β, at the tool-chip interface was 0.67 for Test No. 1. This value was determined from the cutting, F_c, and thrust, F_t, force data reported in Ref. [34] and $\boldsymbol{\beta = (F_t + F_c \tan\alpha)/(F_c - F_t \tan\alpha)}$ where α is the rake angle. Note that some uncertainty in the reported thrust force caused by the cutting edge radius and associated size effect is likely, which subsequently propagates into estimation of β. The coefficient of friction for Test No. 2 was assumed to be 0.5 since the cutting forces were not reported and the tool material was different than in Test No. 1.

Table 3. Orthogonal cutting tests data reported in the literature [33,34]; D_0 is the original grain size, V_c is the cutting speed, *DoC* is the depth of cut, and α is the rake angle.

Test #	Material	D_0 (μm)	V_c (m/min)	DoC (mm)	α (^{o})
1	ETP Cu	47.4	36	0.25	-5
2	OFHC Cu	96±24	28.2	0.21	+20

5. Results and discussion

In the following, the predicted cutting forces and cutting-induced hardness are compared against the

measurements obtained in the orthogonal cutting tests listed in Table 3.

5.1. Cutting forces

In Table 4, average values of the predicted thrust and cutting forces at steady state are compared with the measured forces (Test No. 1) reported in Ref. [34]. It is seen that the cutting and thrust forces are predicted reasonably well and the relatively small error is mainly due to under-prediction of the force components. Some of this discrepancy is expected since the unified material model was calibrated for OFHC copper with larger initial grains (62 μm) and lower impurity than the ETP grade copper used in the orthogonal cutting tests reported in [34]. The lower impurity and larger initial grain size render the OFHC copper mechanically softer than the ETP grade copper and hence, for similar cutting conditions, the predicted cutting and thrust forces would be expected to be a bit lower for OFHC copper.

Table 4. Measured and predicted forces in orthogonal cutting of copper.

Force (N)	Measured [34]	Predicted	Error
F_c	1177	1082	8.1
F_t	945	823	12.9

5.2. Cutting-induced hardness

Figure 2 shows a contour plot of predicted cutting-induced hardness and an overlaid, imaginary grid of measurement nodes for Test No. 1 in Table 3. The hardness measurements reported in [34] were made using a *Knoop indenter* with a *fixed* load of 25 gf. As mentioned before, the data used to calibrate the material model were for OFHC copper, which is softer than the ETP grade copper used in Test No. 1. To compensate for this *initial* discrepancy in the hardness of the model and test materials, the uniaxial strain equivalent of the test material's initial hardness (67.4 ± 12% kg/mm^2) was *estimated* using the hardness data for annealed copper reported by Tabor [31] (*see* Table 2). The latter resulted in an equivalent pre-strain of ~12% which was added to the sum of the predicted and indentation strains in calculating the indentation stress, σ_{in}, in Eqn. (17). This corrective measure, albeit effective in matching the *initial* hardness of the model and test materials, is not expected to entirely eliminate the discrepancy between the predicted and measured hardness as structural defects, particularly point defects such as impurities, have a sizable negative effect on the thermal conductivity of copper and on the ensuing thermal softening during cutting. Thereby, it is anticipated that, under identical cutting conditions, thermal softening will be more pronounced for ETP grade copper than OFHC copper.

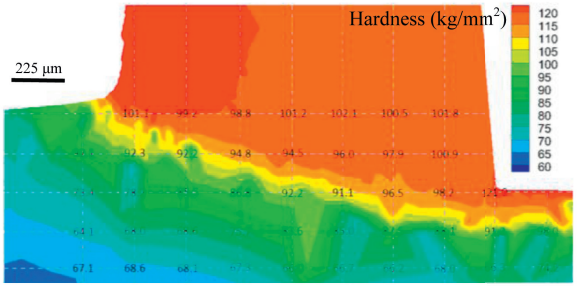

Fig. 2. Comparison between predicted cutting-induced hardness and empirically measured values [34]. Note the numbers at the nodes of the imaginary grid are measured values; model material – OFHC Cu (99.99% pure), test material - ETP grade copper (99.9% pure).

Looking at the evolution trend of the predicted hardness, it is seen that it is very well aligned with the trend exhibited by the work hardening evolution when going from the undeformed material into the primary shear zone and ultimately into the chip. It is noticed that the model over-predicts the hardness in the primary shear zone and in the chip by up to ~17%, which is deemed acceptable considering the reported 5~10% standard deviation in the reported measurements [34] and the foregoing discussion on the pronounced effect of thermal softening for ETP grade copper.

To minimize the effect of material purity on the predicted hardness, a separate simulation was run at the cutting conditions listed in Table 3 for Test No. 2 wherein the test material is reported as OFHC copper (99.99% pure). The model material is also OFHC copper (99.99% pure), albeit with a smaller initial grain size of 62 μm. The hardness measurements reported in [33] were conducted using a *Vickers indenter* with a *fixed* penetration depth resulting in typical diagonal lengths of 35~50 μm to avoid the likely size effects. Here as well, the uniaxial strain equivalent of the test material's initial hardness (56 ± 4 kg/mm^2) was *estimated* using the hardness data for annealed copper reported by Tabor [31] (*see* Table 2). The latter resulted in an equivalent pre-strain of ~5% (another indication of the similarity between the model and test materials), which was added to the sum of the predicted and indentation strains in calculating the indentation stress, σ_{in}, as in Eqn (17).

The reported average chip hardness is 152±5 kg/mm^2 [33], which compares reasonably well with the predicted average chip hardness of 138 kg/mm^2 (~9% discrepancy) (*see* Figure 3). The latter is an improvement of ~8% in hardness prediction compared to the case where the purity levels of the model and test materials were different.

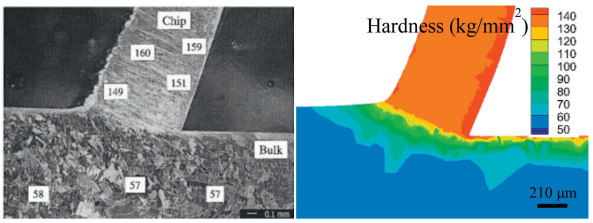

Fig. 3. Comparison between predicted cutting-induced hardness and empirically measured values [33]. Both model and test materials are OFHC copper (99.99% pure).

It is also seen that the cutting-induced hardness is under-predicted in this case, albeit slightly. The most plausible source for this discrepancy, and partly for the over-prediction in the previous case, seems to be the inherent uncertainty in the estimation of the indentation strain, which propagates into the data used to obtain Eqn. (18) for the proportionality parameter C. It is reported that the saturated value of C at large strains (typical of machined surface and chip strains) can vary between 3.0 ~ 3.5 depending on the magnitude of the indentation strain [32].

6. Conclusions

In this study, the machining-induced hardness was predicted using a new material model that describes the constitutive behavior of the material during inelastic deformation explicitly in terms of the underlying microstructure evolution. The average grain size and dislocation density evolutions due to hardening, dynamic recovery, and dynamic recrystallization mechanisms were captured using a set of evolution laws enabling the prediction of hardness evolution on a more physical basis. To evaluate the model's performance in predicting the hardness under steady state chip formation conditions, a set of orthogonal cutting tests were simulated by implementing the unified material model and the hardness model in AdvantEdge™, a commercially-available finite element-based machining simulation code. The cutting forces were predicted with acceptable accuracy. The predicted hardness evolution was very well aligned with the work hardening evolution and the cutting-induced hardness was predicted reasonably well.

Acknowledgements

The authors would like to acknowledge support for this work from a Department of Energy Innovative Manufacturing Initiative award No. DE-EE0005762/000.

References

[1] Brown, T.L., Saldana, C., Murthy, T.G., Mann, J.B., Guo, Y., Allard, L.F., King, A.H., Compton, W.D., Trumble, K.P., Chandrasekar, S., 2009. A Study of the Interactive Effects of Strain, Strain Rate and Temperature in Severe Plastic Deformation of Copper. Acta Materialia 57, p. 5491.

[2] Calistes, R., Swaminathan, S., Murthy, T.G., Huang, C., Saldana, C., Shankar, M.R., Chandrasekar, S., 2009. Controlling Gradation of Surface Strains and Nanostructuring by Large-Strain Machining. Scripta Materialia 60, p. 17.

[3] Ramesh, A., Melkote, S.N., Allard, L.F., Riester, L., Watkins, T.R., 2005. Analysis of White Layers Formed in Hard Turning of AISI 52100 Steel. Materials Science and Engineering A 390, p. 88.

[4] Ramesh, A., Melkote, S.N., 2008. Modeling of White Layer Formation under Thermally Dominant Conditions in Orthogonal Machining of Hardened AISI 52100 Steel. International Journal of Machine Tools and Manufacture 48, p. 402.

[5] Johnson, G.R., Cook, W.H., 1983. A Constitutive Model and Data for Metals Subjected to Large strains, High Strain Rates and high Temperatures. Proceedings of the 7th International Symposium on Ballistics 54, p. 1.

[6] Zerilli, F.J., Armstrong, R.W., 1987. Dislocation-Mechanics-Based Constitutive Relations for Material Dynamics Calculations. Journal of Applied Physics 61, p. 1816.

[7] Zerilli, F.J., Armstrong, R.W., 1998. Dislocation Mechanics Based Constitutive Equation Incorporating Dynamic Recovery and Applied to Thermomechanical Shear Instability. AIP Conference Proceedings 429, p. 215.

[8] Umbrello, D., Hua, J., Shivpuri, R., 2004. Hardness-Based Flow Stress and Fracture Models for Numerical Simulation of Hard Machining AISI 52100 Bearing Steel. Materials Science and Engineering A 374, p. 90.

[9] Umbrello, D., Filice, L., 2009. Improving Surface Integrity in Orthogonal Machining of Hardened AISI 52100 Steel by Modeling White and Dark Layers Formation. CIRP Annals – Manufacturing Technology 58, p. 73.

[10] Umbrello, D., 2011. Influence of Material Microstructure Changes on Surface Integrity in Hard Machining of AISI 52100 Steel. International Journal of Advanced Manufacturing Technology 54, p. 887.

[11] Caruso, S., DiRenzo, S., Umbrello, D., Jayal, A.D., Dillon, O.W., Jawahir, I.S., 2011. Finite Element Modeling of Microstructure Changes in Hard Turning. Advanced Materials Research 223, p. 960.

[12] Yanagimoto, J., Karhausen, K., Brand, A.J., Kopp, R., 1998. Incremental Formulation for the Prediction of Flow Stress and Microstructural Change in Hot Forming. ASME Journal of Manufacturing Science and Engineering 120, p. 316.

[13] Rotella, G., Settineri, L., Umbrello, D., Dillon, O.W., Jawahir, I.S., 2012. Finite Element Modeling of Microstructure Changes in Turning of AA7075-T651 Alloy and Validation. Proceedings of the 40th North American Manufacturing Research Conference. Indiana, USA, paper #7765.

[14] Hughes, G.D., Smith, S.D., Pande, C.S., Johnson, H.R., Armstrong, R.W., 1986. Hall-Petch Strengthening for the Microhardness of Twelve Nanometer Grain Diameter Electrodeposited Nickel. Scripta Metallurgica 20, p. 93.

[15] Sheppard, T., Tunnicliffe, P.J., Patterson, S.J., 1982. Direct and Indirect Extrusion of a High Strength Aerospace Alloy (AA 7075). Journal of Mechanical Working Technology 6, p. 313.

[16] Pu, Z., Umbrello, D., Puleo, D.A., Dillon, O.W., Lu, T., Jawahir, I.S., 2013. Finite Element Modeling of Microstructure Changes in Dry and Cryogenic Machining of AZ31B Magnesium Alloy for Enhanced Corrosion Resistance. Proceedings of the 41th North American Manufacturing Research Conference. Wisconsin, USA, paper #1564.

[17] Ding, H., Shin, Y.C., 2011. Dislocation Density-Based Grain Refinement Modeling of Orthogonal Cutting of Commercially Pure Titanium. Proceedings of the 2011 ASME International Manufacturing Science and Engineering Conference. Oregon, USA, paper #50220.

[18] Estrin, Y., Tóth, L.S., Molinari, A., Bréchet, Y., 1998. A Dislocation-Based Model for All Hardening Stages in Large Strain Deformation. Acta Materialia 46, p. 5509.
[19] Tóth, L.S., Molinari, A., Estrin, Y., 2002. Strain Hardening at Large Strains as Predicted by Dislocation Based Polycrystal Plasticity Model. ASME Journal of Engineering Materials and Technology 124, p. 71.
[20] Lemiale, V., Estrin, Y., Kim, H.S., O'Donnell, T., 2010. Grain Refinement under High Strain Rate Impact: A Numerical Approach. Computational Materials Science 48, p. 124.
[21] Svoboda, A., Wedberg, D., Lindgren, L.E., 2010. Simulation of Metal Cutting Using a Physically Based Plasticity Model. Modeling and Simulation in Materials Science and Engineering 18, p. 075005/1.
[22] Lindgren, L.E., Domkin, K., Hanson, S., 2008. Dislocations, Vacancies and Solute Diffusion in a Physically Based Plasticity Model for AISI 316L. Mechanics of Materials 40, p. 907.
[23] Liu, R., Salahshoor, M., Melkote, S.N., Marusich, T., 2014. A Unified Internal State Variable Material Model for Inelastic Deformation and Microstructure Evolution in SS304. Materials Science and Engineering A 594, p. 352.
[24] Kocks, U.F., Argon, A.S., Ashby, M.F., 1975. Thermodynamics and Kinetics of Slip. Progress of Materials Science 19, p. 139.
[25] Mecking, H., Kocks, U.F., 1981. Kinetics of Flow and Strain-Hardening. Acta Metallurgica 29, p. 1865.
[26] Kocks, U.F., 1976. Laws for Work-Hardening and Low-Temperature Creep. ASME Journal of Engineering Materials and Technology 98, p. 76.
[27] Follansbee, P.S., Gray, G.T., III 1991. Dynamic Deformation of Shock Prestrained Copper. Materials Science and Engineering A 138, p. 23.
[28] Estrin, Y., Mecking, H., 1984. A Unified Phenomenological Description of Work Hardening and Creep Based on One Parameter Models. Acta Metallurgica 32, p. 57.
[29] Liu, R., Salahshoor, M., Melkote, S.N., Subramaniam, J., Marusich, T., 2014. A Unified Approach to Modeling Material Behavior and Microstructure Evolution in Machining of OFHC Copper. Proceedings of the 2014 ASME International Manufacturing Science and Engineering Conference. Michigan, USA, paper #4180.
[30] Beeuwkes, R., Chait, R., Jr., Lin, H.H., 1973. The Practical Determination of Flow Curves by Indentation Hardness Methods, in "*The Science of Hardness Testing and Its Research Applications*" J.H. Westbrook, H. Conrad, Editors. American Society of Metals, Ohio, p. 75.
[31] Tabor, D., 1948. A Simple Theory of Static and Dynamic Hardness. Proceedings of the Royal Society of London A 192, p. 247.
[32] Chaudhri, M.M., 1998. Subsurface Strain Distribution around Vickers Hardness Indentations in Annealed Polycrystalline Copper. Acta Materialia 46, p. 3047.
[33] Brown, T.L., Swaminathan, S., Chandrasekar, S., Compton, W.D., King, A.H., Trumble, K.P., 2002. Low-Cost Manufacturing Process for Nanostructured Metals and Alloys. Journal of Materials Research 17, p. 2484.
[34] Elmadagli, M., Alpas, A.T., 2003. Metallographic Analysis of the Deformation Microstructure of Copper Subjected to Orthogonal Cutting. Materials Science and Engineering A 355, p. 249.